Original Article

Quantum Computing Analysis of Naphthalene Compound: Electronic Structure, Optical, and Thermochemical Approaches using DFT and HF

Othman Abdulrahman Hamad[a] | Rebaz Obaid Kareem[b,*] | Yousif Hussein Azeez[b] | Mehmet Hanifi Kebiroğlu[c] | Rebaz Anwar Omer[d] | Osama Ismail Haji Zebari[e,f]

[a]*University of Raparin, College of Science, Department of Chemistry, 46012, Sulamani, Iraq*
[b]*Physics Department, College of Science, University of Halabja, 46018, Halabja, Iraq*
[c]*Department of Opticianry, Darende Bekir Ilicak Vocational School, Malatya Turgut Ozal University, Malatya, Türkiye*
[d]*Koya University, Faculty of Science & Health, Department of Chemistry, Koya KOY45, Kurdistan Region – F.R., Iraq*
[e]*General Science Department, Faculty of Education, Soran University, Soran 44008, Iraq*
[f]*Medical Biochemical Analysis Department, College of Health Technology, Cihan University-Erbil, Kurdistan Region, Erbil 44008, Iraq*

Use your device to scan and read the article online

Citation O.A. Hamad, R.O. Kareem, Y.H. Azeez, M.H. Kebiroğlu, Rebaz Anwar Omer, O.I. Haji Zebari, **Quantum Computing Analysis of Naphthalene Compound: Electronic Structure, Optical, and Thermochemical Approaches using DFT and HF.** *J. Appl. Organomet. Chem.*, **2024**, *4*(2), 100-118.

https://doi.org/10.48309/JAOC.2024.444132.1167

Article info:
Submitted: 17 February 2024
Revised: 29 February 2024
Accepted: 17 March 2024

ID: JAOC-2402-1167
Checked for Plagiarism: Yes
Language Editor Checked: Yes

Keywords:
Naphthalene, DFT, HF, Optical properties, Thermochemistry, DOS

ABSTRACT

The novelty of the work lies in the application of quantum computing analysis, specifically employing density functional theory (DFT) and Hartree-Fock (HF) techniques with various basis sets (aug-cc-pVQZ, 3-21G, 6-31G, 6-311G, and SDD), this work examined the structure and characteristics of naphthalene. The theoretical nature of naphthalene's structure and characteristics: Highest Occupied Molecular Orbital (HOMO), Lowest Unoccupied Molecular Orbital (LUMO), band gap BG, density of state (DOS), Ultraviolet (UV), and Natural Bond Orbital (NBO) are explored. Several additional characteristics have been studied: thermochemical properties at standard temperature and pressure, and their optical properties (Optical BG with the indirect and direct transition). The DFT/aug-cc-pVQZ basis was used with a fixed value of 4.75 eV to determine the HOMO-LUMO gap of naphthalene in this investigation. We find that the gaps of 4.71, 4.873, and 4.74 eV, respectively, in a recent density-functional theory (DFT) study that agrees with our results.

Introduction

Naphthalene (NPH) is the most prevalent among the polycyclic aromatic hydrocarbons observed in polluted urban settings and has been identified in air environments. Being exposed to elevated levels of (NPH) could lead to negative impacts on health, potentially even leading to cancer development in humans [1]. NPH is a chemical compound with several other names. It is often referred to as Naphthene, Naphthalin, Camphor tar, White tar, and Albocarbon. It is a white crystalline solid and the simplest polycyclic aromatic hydrocarbon. In 1819, a Scottish scientist named Alexander Garden developed naphthalene. In 1826, its chemical formula ($C_{10}H_8$) was originally

***Corresponding Authors: Rebaz Obaid Kareem** (obedrebaz9@gmail.com)

published by Michael Faraday [2]. The NPHs are a self-organizing class of small, electron-deficient aromatic compounds [3]. NPH is the simplest and most fundamental member of the arenas family and is formed by the ortho fusion of two benzene rings. NPH is a substance that melts at 82.2 ◦C and generates glistening flakes of crystal. The smell of mothballs is unmistakable. Extremely fugitive, and slowly sublimes at room temperature, it is the most volatile of the polycyclic aromatic hydrocarbons because of its bicyclic aromatic structure [4-6]. In contrast to its insolubility in water, it is very marginally soluble about (32 mg/L), has a relatively high solubility in alcohol, ether, and benzene. Naphthalene and isomers structural are common air pollutants in defunct coal and oil gasification facilities, with NPH concentrations more than 10 times greater than any other polycyclic aromatic hydrocarbons found. It produces a hazy flame when lit [7]. Naphthalene is mostly produced by the combustion of gasoline and diesel. Major emission sources of NPH include the burning of fossil fuels and wood. For both gasoline and diesel fuels, NPH was shown to be the most common PAH in the research conducted by Marr *et al.* (1999). The majority of NPH found in car exhaust comes from either unburned gasoline or the oxidation of 2-methylnaphthalene included in the fuel itself [8]. NPH compounds are widespread because they are used in many everyday items, including textile dyes, consumer goods, insecticides, plasticizers, and tanning agents. Likewise, they can be synthesized by maleic anhydride reacting with 1,1 diaryl ethylene in a Diels-Alder reaction, and the resulting bis product is aromatized by decarboxylation with barium hydroxide and copper. Wagner-Jauregg reaction also creates naphthalene with a phenyl replacement [9]. NPH has eight protons, so ^{1}H-NMR spectrum displays two distinct kinds of peaks. Downfield, you can see the ring's protons, and at δ 7.32 and δ 7.67, you will see a doublet of around eight protons. Three distinct forms of carbon are seen in the ^{13}C-NMR spectra of naphthalene. The ^{13}C spectrum has peaks at 133.6 for carbons 4a and 8a, 125.9 for carbons 2, 3, 6, and 7, and 128.6 for carbons 1, 4, 5, and 8. NPH molecules have a D_2h symmetric, planar, bihexagonal, catacondensed structure. There are essentially 48 different vibrations [10-12]. This structural combined effect stabilizes of NPH at a resonance energy of 61 kcal/mol. Both the alpha (1, 4, 5, and 8) and beta (2, 3, 6, and 7) places are filled by hydrogen atoms, making up the two sets of equivalents. Carbon-carbon bonds are shorter than expected, as shown by X-ray diffraction, carbon-carbon bonds are on average 1.42 (142 p.m.) in length, whereas the length of bonds C1, C2, C3, C4, C5, and C7, C8 is around 1.37 (137 p.m.) [2]. Naphthalene is among the numerous nonionic organic pollutants detected in both air and soil [13]. NPH has been found to induce DNA damage and lipid peroxidation in cells, and its exposure has been linked to anemia in both humans and dogs, as well as severe lung tissue necrosis in mice. In addition, studies involving rabbits, mice, and rats have also shown adverse effects [14,15]. Naphthalene is a cytotoxic moiety that has been studied extensively as a conjugated aromatic system for treating a wide range of pathophysiological conditions, including cancer, infection, inflammation, virus, tuberculosis, hypertension, diabetes, neurodegeneration, psychosis, convulsions, and depression. The deadly effect of naphthalene is due to its most reactive metabolites, naphthalene epoxides, and naphthoquinones, which form covalent bonds with the cysteine amino acid in proteins found in cells. Several naphthalene-containing medicines, including nafcillin, naftifine, tolnaftate, terbinafine, etc. are available and serve an important role in the prevention and treatment of microbial infection. The antibacterial action of the coloring ingredient ß-naphthol is particularly effective [16].

This work predicts and analyzes the molecular geometry properties of naphthalene, including HOMO, LUMO, BG, DOS, UV, and NBO, as well as its thermochemical and optical properties. The application of quantum computing analysis is novel, specifically using density functional theory (DFT) and Hartree-Fock (HF) techniques with various basis sets (aug-cc-pVQZ, 3-21G, 6-31G, 6-311G, and SDD). The structure and characteristics are reviewed.

Experimental

Computational study

The use of the Gaussian 09W program suite in the investigation of the naphthalene molecule's structure. DFT and HF were the two favored approaches. Hartree-Fock (HF) and density functional theory (DFT) are both short forms for other words. For each of these two methods, we optimized the structure by choosing the basis sets on their own. Based on these findings, various basis sets have been uousid (STO-3G, 3-21G, 6-31G, 6-311G, and SDD). Because it is a polarized double-zeta basis set, polarization functions are included for each atom in this set. The study found that the structure of naphthalene was best predicted using this approach. Compared to the experimental data, the calculated bond lengths and angles were quite close [17-23]. Good agreement was found between the predicted and experimental HOMO-LUMO gap. Conclusions the DFT basis set was shown to be appropriate for investigating naphthalene's structure and electronic characteristics [24,25]. By conducting single-point calculations, we were able to evaluate both the overall and localized characteristics of the optimized molecules. It is important to note that certain factors have a significant influence on the reactivity of chemicals. The following parameters are commonly identified as eigenvalues representing various energy-related properties: E_{HOMO} (Highest Occupied Molecular Orbital Energy), E_{LUMO} (Lowest Unoccupied Molecular Orbital Energy), the energy band gap (E_{gap}), ionization energy (IE), electron affinity (EA), absolute electronegativity (χ), global hardness (η), global softness (S), global electrophilicity (ω), electroaccepting *ω*+, electrodonating *ω*-, the fraction of electrons transferred, [26-28] and the maximum fraction of electrons transferred (ΔN_{max}). Neutrality is defined by the difference between IE and EA, or cation and anion, respectively. By solving Equations (**1**) and (**2**), we were able to get the ionization energy and electron affinity [29]:

$$IE = E(N-1) - E(N) \quad (1)$$

And

$$EA = E(N) - E(N+1) \quad (2)$$

Here we designate the energy (E) of the neutral by (N), that of the cation by (N-1), and that of the anion by (N+1). The band gap energy, denoted by the symbol (E_{gap}), is the difference in energy that exists between the two states denoted by E_{LUMO} and E_{HOMO} as, as shown in Equation (**3**) [30]:

$$\Delta E_{Gap}(eV = E_{HOMO} - E_{LUMO}) \quad (3)$$

Equation (**4**) was used to get the absolute chemical hardness [30]:

$$\eta = \frac{IE - EA}{2} = \frac{E_{HOMO} - E_{LUMO}}{2} \quad (4)$$

In Equation (**5**), molecular softness characterizes an atom or set of atoms' electron-receiving areas [30]:

$$S = \frac{1}{\eta} = \frac{2}{E_{LUMO} - E_{HOMO}} \quad (5)$$

As seen in Equation (**6**), the negative value of the chemical potential, or, contributes the χ is a significantly to the total reactivity [30]:

$$\chi = \frac{IE + EA}{2} = \frac{-(E_{HOMO} + E_{LUMO})}{2} \quad (6)$$

Equation (**7**) is the formula that is used to calculate the electronic chemical potential based on the electronic molecular orbital (EMO) energies.

$$\mu = \frac{E_{HOMO} + E_{LUMO}}{2} \quad (7)$$

Using Equation (**8**), the magnitude of the greatest energy drop was obtained that occurred as a direct consequence of the movement of electrons from the donor to the acceptor. In addition, the global electrophilicity (***ω***) index of a chemical species is obtained by the process of dividing the square of the electronegativity (***χ***) by the chemical hardness. This definition was provided by Parr and colleagues [29]:

$$\omega = \frac{\mu^2}{2} \times S = \frac{\mu^2}{2\eta} \quad (8)$$

Electrons that were donated and accepted were determined using Equations (**9**) and (**10**) [30]. Where, $\boldsymbol{\omega}^+$ (+) represents the system's ability

to take in charges and ω^- (-) indicates that it can give them out to other molecules.

$$\omega^+ = \frac{EA^2}{2(IE - EA)} \quad (9)$$

$$\omega^- = \frac{IA^2}{2(IE - EA)} \quad (10)$$

We observe that a higher value for ω^+ signifies that a system may absorb charge (accept charge), while a lower value for ω^- suggests that it is a more efficient electron donor. Equation (11) was used to calculate the greatest amount of electrons an electrophile may get via the application of the quantum chemical method [30]:

$$\Delta N_{max} = \frac{-\mu}{\eta} \quad (11)$$

Gauss View 6.0 is a piece of software for molecular modeling that may be used to fine-tune the molecular structure. It may be used to determine molecular attributes such as vibrational wave numbers in addition to energy, which is determined in several different ways. NMR, UV, and FTIR spectra are all examples of experimental methods that may be used to learn about the internal structure and external characteristics of molecules. NMR spectroscopy may be used to find out how many atoms are in a molecule, what kinds of atoms are in it, and how they are connected [31]. An element's electronic configuration may be established by ultraviolet (UV) spectroscopy. It is possible to learn a molecule's vibrational frequencies through FTIR spectroscopy. Calculating a molecule's DOS spectrum is a breeze with the help of the Gauss Sum application. The density of states (DOS) spectrum is the energy-versus-state-number diagram. One may use it to learn about the vibrational modes of a molecule and how their energies compare to one another [32-34].

Results and Discussion

Geometry optimization

The optimized ground energies of Naphthalene molecules are shown in Figure 1. B3LYP/6- 31G base sets were used to improve geometry in a more complicated setting. However, methods such as the Molecular Mechanics approach, Density Functional Theory (DFT), and the Hartree-Fock method are used to find the most effective configuration for a chemical. The structure of naphthalene was optimized in this work using density functional theory and hydrogen bonding. Determining the energy associated with a certain initial molecule shape is the initial step in a geometry optimization technique that may be useful for this strategy.

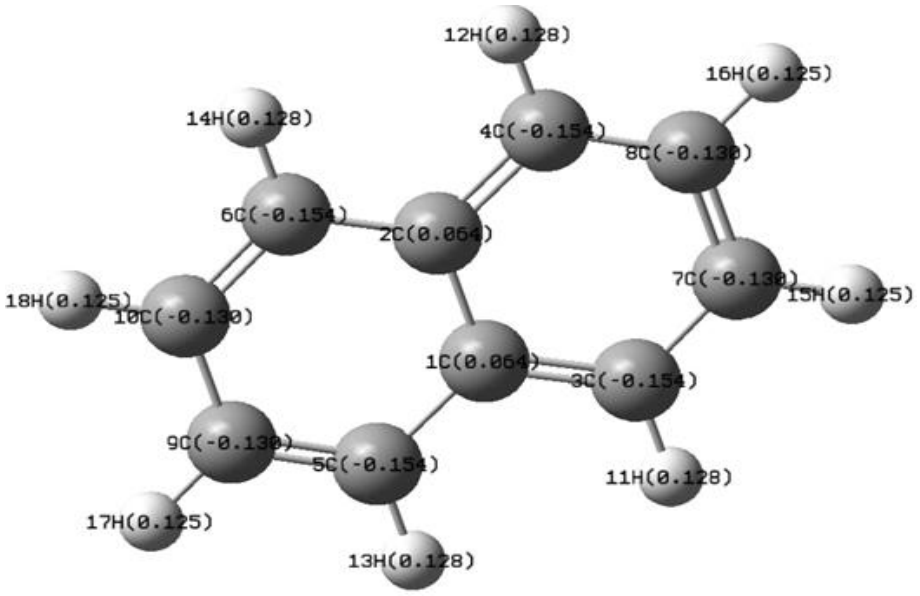

Figure 1. Geometrical optimization naphthalene

Natural bond orbital (NBO) analysis

NPH has a Color Range of 1.087 to 1.442. NPH molecules include 10 carbon atoms and 8 hydrogen electrons, which gives the substance a white solid crystalline appearance and the molecular formula ($C_{10}H_8$). NPH gas is a known irritant to the respiratory system, skin, and eyes. It is a key ingredient in a wide variety of goods, including pesticide carbonyls, polymers, leather tanning agents, and colors. Structures of naphthalene compounds that have been tuned for performance are shown in Figure 2. Furthermore, it is shown and diffraction the length bonds of Carbon-carbon bonds (C2-C3, C1-C10, C5-C6, and C7-C8) =1.389 p.m. are shorter than carbon-carbon bonds (C1-C2, and C6-C7) =1.429 p.m. and shorter than carbon-carbon bonds (C3-C4, C4-C5, C8-C9, and C9-C10) =1.431 p.m. A bout Hydrogenes (H11, H12, H15, and H16) =1.087 p.m. shorter than (H13, H14, H17, and H18) =1.088 p.m. Initial Parameters (Angstroms and Degrees) are indicated in Table 1.

Thermochemistry

The comprehension of naphthalene's behavior in many applications, such as chemical reactions, phase transitions, and thermal processes, necessitates a thorough understanding of its thermodynamic properties and parameters. It has been shown that energy distribution and thermal qualities are greatly affected by normal conditions of 298.150 K and 1 atm pressure in thermochemistry. The system's total thermal energy (E) is determined to be 97.63 kcal/mol, with a heat capacity at constant volume (Cv) of 28.23 cal/mol K and entropy (S) of 78.87 cal/mol K. Remarkably, the electronic contribution to the system's energy, heat capacity. Entropy is found to be negligible,

Table 1. Initial parameters (angstroms and degrees)

Definition	Length (Å)	Definition	Length (Å)
C1-C2	1.4288	C5-H14	1.0884
C1-C10	1.3889	C6-C7	1.4288
C1-H11	1.0874	C6-H15	1.0874
C2-C3	1.3889	C7-C8	1.3889
C2-H12	1.0874	C7-H16	1.0874
C3-C4	1.4311	C8-C9	1.4311
C3-H13	1.0884	C8-H17	1.0884
C4-C5	1.4311	C9-C10	1.4311
C4-C9	1.4423	C10-H18	1.0884
C5-C6	1.3889	-	-

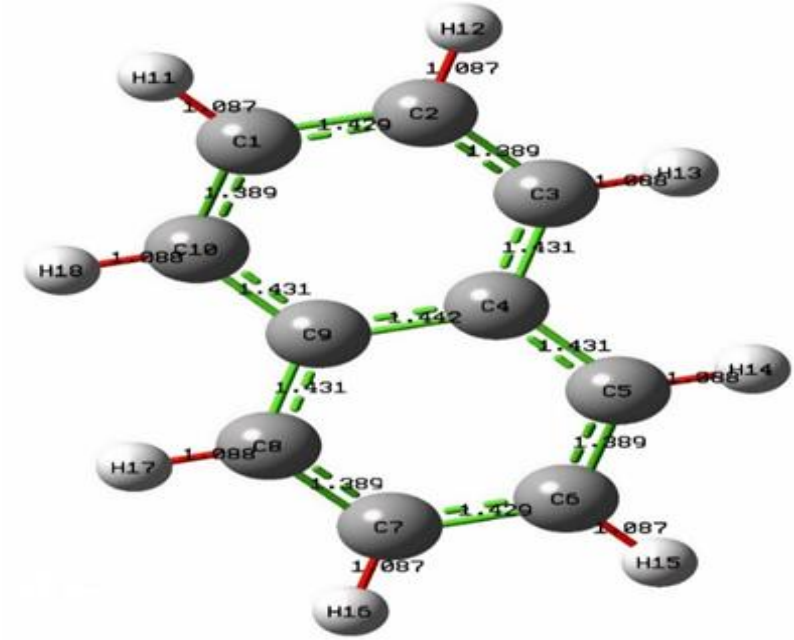

Figure 2. Naphthalene color range from 1.087 to 1.442

signifying the dominance of other degrees of freedom. The translational and rotational degrees of freedom contribute modestly to both Cv and S, with values of 0.889 kcal/mol, 2.981 cal/mol K, and 40.45 cal/mol K for translational energy, translational Cv, and translational entropy, respectively. Similarly, rotational parameters yield values of 0.889 kcal/mol, 2.981 cal/mol K, and 26.23 cal/mol K for energy, Cv, and entropy, respectively.

In contrast, the vibrational contribution to the point is notably substantial at 95.85 kcal/mol, while its impact on Cv and S is also significant, with values of 22.27 cal/mol K and 12.19 cal/mol K, respectively. These findings collectively underscore the importance of vibrational modes in contributing to the system's thermal properties, providing valuable insights into the system's thermodynamic behavior under standard conditions. According to Table 2, the enthalpy (ΔH), specific heat capacity (Cv), and entropy are shown at ambient conditions.

Band gap energy

The theoretical effectiveness of inhibitors and static molecular reactivity are both affected by the energy gap between E_{HOMO} and E_{LUMO}. ΔE comparisons are helpful in inhibitor research since the stronger the inhibition, the smaller the energy distances. The E_{HOMO} is more closely connected to the found ΔE value than the E_{LUMO}, which is currently employed in corrosion inhibitors research. The inhibitor derivatives may serve as anti-corrosion chemicals because of their high HOMO energy and low ΔE. The largest HOMO energy and lowest ΔE value suggest that the chemical in question has a strong inhibitory effect. In contrast to atoms, molecules do not share the same orbitals. BG energy is the difference in potential energy between the (HOMO) and (LUMO) states of a molecule. In this study, we have analyzed the performance of many distinct sets of basis groups at a wide range of BG energy levels, as demonstrated in Figure 3.

The global reactivities are strongly linked to the corrosion resistance, chemical reactivity, stability, and inhibitor resistance of compounds. The HOMO and LUMO energies were initially calculated using Density Function and Hartree Fock theory with various basis sets, as presented in Table 3. Based on the findings of this research, the **aug-cc-pVQZ** basis set possesses a higher HOMO energy of (-6.13eV). and the 6-31G basis set lower value (-5.82 eV). This shows that it is compatible with low-energy acceptor molecules that have unoccupied molecular orbitals and that it has a predisposition to give electrons. In this current study, for instance, the HOMO-LUMO gap of naphthalene was computed using DFT/ aug-cc-pVQZ basis with a fixed value of 4.75 eV.

Table 2. Thermochemistry using standard temperature 298.150 K, and 1 atm. pressure

Calculation of Parameters	E (Thermal) kcal/mol	Cv cal/mol.K	S cal/mol.K
Total (Energy)	97.63	28.23	78.87
Electronic (Energy	0.000	0.000	0.000
Translational (Energy)	0.889	2.981	40.45
Rotational (Energy)	0.889	2.981	26,23
Vibrational (Energy)	95.85	22.27	12.19

Table 3. HOMO, LUMO energy using DFT, HF methods to naphthalene compound

Bais sets	DFT			HF		
	HOMO	LUMO	BG (eV)	HOMO	LUMO	BG (eV)
aug-cc-pVQZ	-6.13	-1.37	4.75	-7.99	1.04	-9.03
3-21G	-5.91	-0.96	4.94	-9.25	-5.17	-4.08
6-31G	-5.82	-0.96	4.86	-9.27	-5.90	-3.37
6-311G	-6.07	-1.21	4.85	-9.22	-5.46	-3.75
SDD	-5.98	-1.21	4.76	-9.25	-5.17	-4.08

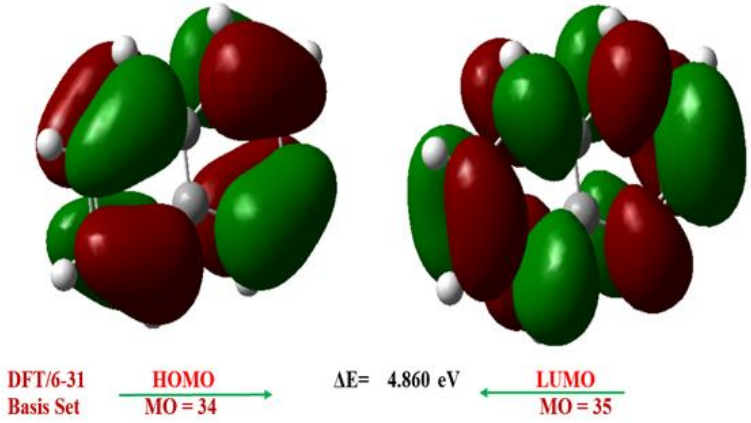

Figure 3. HOMO, LUMO energy diagram naphthalene compound, using DFT method

This is in compared to a recent DFT research that found the gap to be 4.71 eV, and TD-DFT investigation that found the gap to be 4.74 eV. A molecule with large HOMO–LUMO gap is a hard molecule and with small HOMO–LUMO gap a soft molecule being more reactive. The present research's HOMO-LUMO energy is in conform with a previous DFT investigation on a naphthalene molecule 4.823 eV [17]. A useful metric for predicting the stability and activity of molecules is the LUMO energy gap (Eg). The capacity of the molecule to transport electrons is often inextricably linked to the energy of the HOMO level. Bioactivity may be affected and enhanced by molecules having a small energy gap because of their strong chemical reactivity, and less stability. However, the 3-21G basis set had the largest energy gap, suggesting a much better degree of stability and reduced chemical reactivity in comparison to the other basis sets.
The HOMO is an essential component in corrosion research due to its connection to electron donating ability. As HOMO levels increase, inhibitor chemicals have a larger inhibitory effect.

Ionization energy (IE) and electron affinity (EA)

The IE and EA values determined through the use of the various methods of DFT and HF are presented in Table 4 and Figure 4a. We are particularly interested in the HOMO and LUMO energies to see whether there are any relationships with other, more intriguing molecular/atomic features and chemical values.

Koopmanns' theorem relates the (E_{HOMO}) to the IP, and the (E_{LOMO}) has been used to determine the electron affinity (EA) in straightforward applications of molecular orbital theory. With -E_{HOMO} ≈ IP and E_{LUMO} ≈ EA, the electronegativity (χ) is defined by Mulliken as χ = (IP + EA)/2, where IP and EA are the HOMO and LUMO ionization potential and ionization energy, respectively. The electron donor nature of a substance can be inferred from its small ionization potential values as shown LanL2MB basis set, (4.254 eV). Also, the highest EA value, proves that it is capable of acting as an electron acceptor 6-311G, (6.07 eV).

Hardness (η) and softness (S)

The global hardness and softness of the investigated reagent are illustrated in Figure 4b. Knowledge of the global hardness (η) and softness (S) of a molecule is essential for comprehending its stability and reactivity.
The term "chemical hardness" is used to characterize the charge transfer resistance of a

Table 4. IE, EA energy to Naphthalene using DFT and HF

Basis Sets	DFT		HF	
	IE (eV)	EA (eV)	IE (eV)	IE (eV)
aug-cc-pVQZ	6.13	1.37	7.99	-1.044
3-21G	5.911	0.962	9.25184	5.170147
6-31G	5.826	0.96	9.27905	5.904852
6-311G	6.07	1.215	9.22463	5.469471
SDD	5.982	1.218	9.25184	5.170147

Table 5. Molecular hardness and softness

Basis Sets	DFT		HF	
	η	S	η	S
aug-cc-pVQZ	2.37	0.42	4.51	0.22
3-21G	2.4745	0.404122	2.040848	0.489993
6-31G	2.433	0.411015	1.687101	0.592733
6-311G	2.4275	0.411946	1.87758	0.532601
SDD	2.382	0.419815	2.040848	0.489993

system and evaluate its chemical reactivity. When the values are small, electron transfer is more likely to occur. Energy gaps are usually larger for stiff molecules and smaller for soft ones. Naphthalene ($C_{10}H_8$) was discovered to have the greatest hardness 0.42 eV in the 3-21G / DF, and HF approach. While 2.47 the highest softness is 0.42 in the aug-cc-pVQZ basis set in the current investigation. This suggests that the energy band gap and molecule hardness are closely related and that a greater molecular hardness corresponds to a lower molecular softness (the large band gap causes low molecular softness). The Naphthalene molecule is the most reactive because it has the lowest hardness (η =2.371eV) and the greatest softness (S = 0.42 eV) of the molecules studied. As listed in Table 5. Based on this information, it seems that the aug-cc-pVDZ/DFT and 6-31G/ are softer, naphthalene molecule has the lowest stability, and exhibits a higher level of reactivity.

Global electrophilicity (ω) and the nucleophilicity index (N)

Electrophilicity (ω) is the tendency of a species to accept electrons, but Nucleophiles (N) are species that have excess electron density and can donate electrons to other species, typically in a chemical reaction. An empirical nucleophilicity measure for weak contacts has been further developed recently. By considering both nucleophile and electrophile border orbitals, a new nucleophilicity index is derived. For arines, amines, alcohols, etc. such an index has been used and confirmed using experimentally obtainable kinetic data. The availability of empirical scales of (ω) and (ω^+) has proven extremely helpful in justifying many aspects of chemical difficulties, including selectivity, reaction processes, solvent, and substitute effects. Naphthalene ($C_{10}H_8$) compound, shows that both the DFT and HF methods utilize seven different basis sets. In both methods, the highest values are observed for the cc-pVQZ basis set: electrophilicity (9.79), electrodonating (3.95), electroaccepting (020), and ΔN_{max} (2.80).

Specifically, electrophilicity and electrodonating share the same basis set. It is possible to estimate the projected ranking of chemical stability and reactivity by analyzing the nucleophilic characteristics of the molecules that are being investigated: cc-pVDZ > SSD > 6-311G > 3-21G > 6-31G. High nucleophilic molecules effectively reduce corrosion Examining the electroaccepting, denoted by (ω^+) the symbol, and electrodonating, denoted by the symbol (ω^-), indices that are presented in Table 7. Therefore, a greater value of ω^+ correlates to a stronger capacity of getting a charge, whereas a lower value of ω^- value of a system makes it an excellent electron donor. The molecules are seen as electron donors if the value of ΔN is positive. On the other hand, molecules that function as electron receivers are indicated by a negative value of ΔN. The largest value transfer electrons (ΔN) of naphthalene compound, are directly associated large molecular softness, and small energy gap.

Chemical electron potential (Pi) and electronegativity (χ)

There is a strong linear link between the computed HOMO energies experimental, and calculated ionization potential (IPs), as has been shown. There is a linear relationship between the calculated LUMO energies experimental, and calculated electron affinity (EAs) (for the bound anionic states), the avarage
HOMO/LUMO energies and values, the HOMO-LUMO energy gaps and values, and the HOMO-LUMO and experimental/calculated first excitation energies. The ability of an atom or molecule to attract an electron from another atom or molecule is referred to as its electronegativity, symbolized by the Greek letter **(χ)** [35, 36].

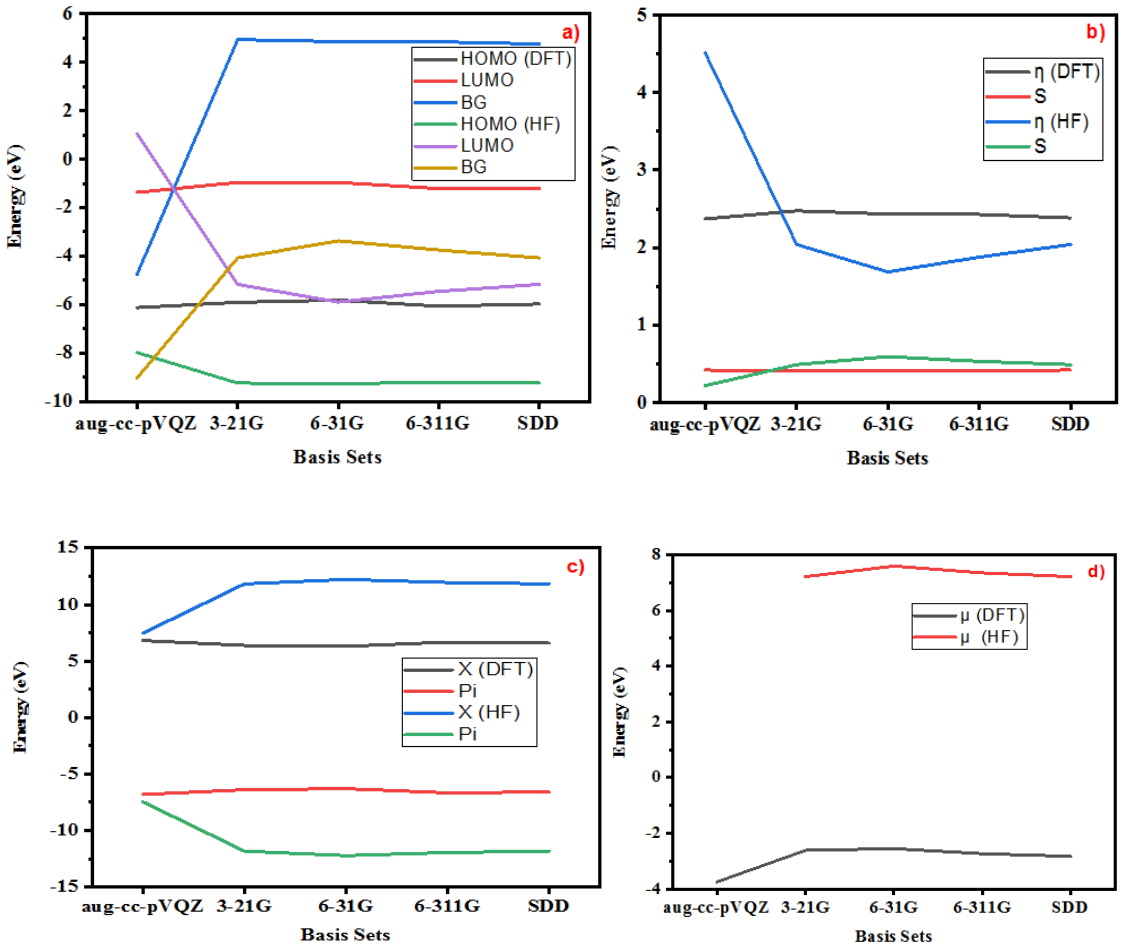

Figure 4. Global reactivity a) HOMO-LUMO, b) hardness and softness, c) chemical electron potential, and electronegativity, and d) dipole moment

Table 6. Electronic potential, electronegativity to naphthalene compound

Basis Sets	DFT		HF	
	X	**Pi**	***X***	**Pi**
aug-cc-pVQZ	6.82	-6.82	7.47	-7.47
3-21G	6.392	-6.39	11.83	-11.83
6-31G	6.306	-6.30	12.23	-12.23
6-311G	6.6775	-6.67	11.959	-11.95
SDD	6.591	-6.59	11.836	-11.83

Table 7. Value of the global electrophilicity (ω), electroaccepting (ω^+) electrodonating (ω^-), and ΔN_{max}

Basis Sets	DFT				HF			
	ω	**ω+**	**ω-**	**ΔNmax**	**ω**	**ω+**	**ω-**	**ΔNmax**
cc-pVQZ	9.79	0.20	3.95	2.8	6.18	0.05	3.53	1.65
3-21G	8.25	0.09	3.52	2.58	34.32	3.27	10.48	1.23
6-31G	8.17	0.09	3.48	2.59	44.33	5.16	12.75	1.22
6-311G	9.18	0.15	3.79	2.75	38.08	3.98	11.33	1.28
SDD	9.11	0.15	3.75	2.76	34.32	3.27	10.48	1.32

The amount of energy necessary to either add or remove an electron from a system is referred to as its electron chemical potential (Pi). The electronic chemical potential, in conjunction with the electron density, is responsible for determining how the electrons in the system are ordered [37].

Table 6 for the naphthalene ($C_{10}H_8$) molecule presents data indicating that both the DFT and HF methods employ seven distinct basis sets. A compounds that have high electronegativity operate as electron capture or suffer a reduction in chemical reactions at the gas phase. The predictive electron capture effectiveness obtained by electronegativity aug-cc-pVQZ > 6-311G > SSD > 3-21G > 6-31G using DFT approach. The electronegativity is shown in Table 2 as a higher rate of electron capture in the **aug-cc-**pVDZ/ DFT/ and 6-31G/HF method. The negative chemical potentials are indicative of their stability suggesting that these do not undergo decomposition into elements. Because of significant electrostatic forces, aug-cc-pVQZ that have high electronegativity operate as electron capture or suffer a reduction in chemical reactions at the gas phase. In Figure 4c, the chemical potential and electronegativity graph of naphthalene was examined using the DFT and HF methods.

Dipole moment (μ)

The dipole moment (μ) is a property of a molecule that measures the overall distribution of electric charge within the molecule. It quantifies the separation of positive and negative charges in a molecule and provides information about the molecule's polarity. In simple terms, it tells you how unevenly the electrons are distributed in a molecule, which is crucial in understanding its behavior in various chemical processes. Table 8 indicates that when employing the DFT method, naphthalene ($C_{10}H_8$) exhibits its highest values (-3.75 C.m) using the aug-cc-pVQZ basis set. when compared to earlier research, this finding was completely in agreement with the earlier research that was conducted on the energy evaluation of the naphthalene molecule's dipole moment, which came in at -3.39 C.m, as shown in Figure 4d.

FT-IR vibrational spectroscopic analysis

Predictions of the vibrational frequencies of our materials for the C-C, and C-H groups were made using the DFT technique, as shown in Table 9, and the results of the IR measurements done on Naphthalene are displayed the IR results showed that the C-H stretching vibration peak for the $C_{10}H_8$ structure occurred between (3000 to 3250 cm^{-1}). The vibrational band diagram was used to build the model of the molecule. FT-IR spectra for this compound: 3200 cm^{-1} (aromatic C-H str); 1550 cm^{-1} (aromatic C=C str, or C-C str); 950 cm^{-1} (C-H bend). 770 cm^{-1} C-H bend. Aromatic between (900-675 cm^{-1}), as shown in Figure 5.

Table 8. Molecular dipole moment

Basis Sets	DFT	HF
	μ (C.m)	μ (C.m)
aug-cc-pVQZ	-3.7500	-3.47677
3-21G	-2.6185	7.210995
6-31G	-2.5535	7.591953
6-311G	-2.738	7.347051
SDD	-2.8315	7.210995

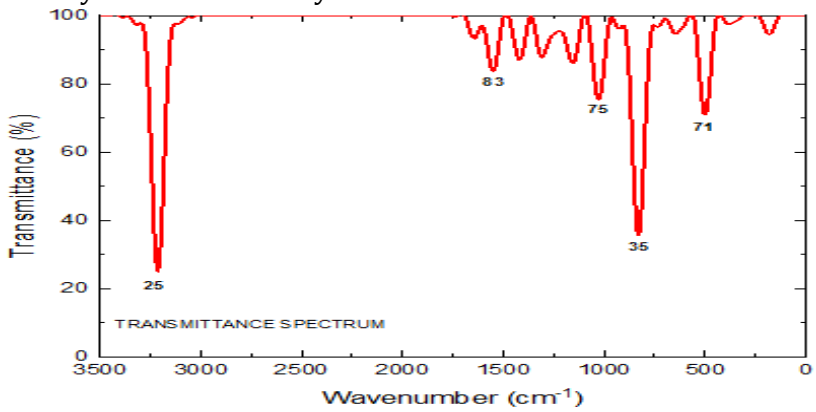

Figure 5. FT-IR vibrational spectroscopic

Table 9. Peak information for naphthalene using FT-IR

Wavenumber (cm-1)	epsilon;(M -1 cm-1)	Wavenumber (cm-1)	epsilon;(M -1 cm-1)
181.3107	75.1537	1048.9779	0
192.12	0	1156.316	33.9306
366.1084	15.974	1181.4965	75.1537
402.747	0	1202.1318	0
491.2868	0	1204.9933	5.25135
499.575	235.188	1247.8417	0
520.2619	0	1287.6749	10.5115
520.6199	0	1308.5156	0
639.5929	22.3392	1414.5858	25.5858
650.7619	0	1421.2448	5.65645
757.7221	0	1441.3244	18.7110
769.0424	0	1490.0504	0
810.6291	0.0004	1492.2063	0
814.5739	0	1552.4577	0
830.1179	852.37	1624.2451	32.1678
881.694	0	1641.3376	0
937.2125	0	1682.302	10.9558
954.9572	0	3183.5486	0
994.9478	0	3185.186	0
1020.4549	36.944	3188.5032	7.46581
1032.3305	0	3191.5483	1.78981
1035.0778	38.9204	3206.4004	0
1040.2132	0	3208.1686	0

Nuclear magnetic resonance spectroscopy

Nuclear magnetic resonance spectroscopy (NMR spectroscopy) is a method that may be used to analyze organic compounds and learn more about their composition and structure. For forecasting NMR spectra and exploring the connection between molecule structure and chemical shifts, quantum chemical calculations are adequate. In the current study DFT technique has been used. As a consequence, it is very useful to learn about and predict molecular structure using a blend of experimental and theoretical methods. Theoretical ^{1}H- and ^{13}C-NMR spectra were estimated using the Gaussian software, and the geometry of the titled chemical was optimized using a typical gauge-including atomic orbital (GIAO) technique [38]. The measured chemical shifts in DMSO d6 varied from 0.00 to 8.00 ppm (Figure 6) while in this study theoretical shifts in the gas phase ranged from 20.00 to 65.00 ppm.

Naphthalene's hydrogen (H) was theoretically identified as a more-than-doublet peak at (24.6644 and 24.8365) ppm in ^{1}H-NMR spectra. This hydrogen's predicted proton resonance signal in the gas phase was measured to be about 24.00 ppm using the DFT technique. The Gaussian software was employed to perform ^{13}C-NMR analysis, revealing the chemical shift values of various carbon atoms within the Naphthalene molecule. The ^{13}C-NMR resonance signals were determined to be 57.4143 ppm for both C4 and C9, and 60.3957 ppm for C3, C5, C8, and C10, respectively. As shown in Table 10, their anticipated values in the gaseous phase were 62.4579 ppm for all C1, C2, C6, and C7 carbon atoms.

Table 10. Chemical shifts of naphthalene using NMR

Method	Shielding (ppm)	Method	Shielding (ppm)
13-H	24.6644	9-C	57.4143
14-H	24.6644	3-C	60.3957
17-H	24.6644	5-C	60.3957
18-H	24.6644	8-C	60.3957
11-H	24.8365	10-C	60.3957
12-H	24.8365	1-C	62.4579
15-H	24.8365	2-C	62.4579
16-H	24.8365	6-C	62.4579
4-C	57.4143	7-C	62.4579

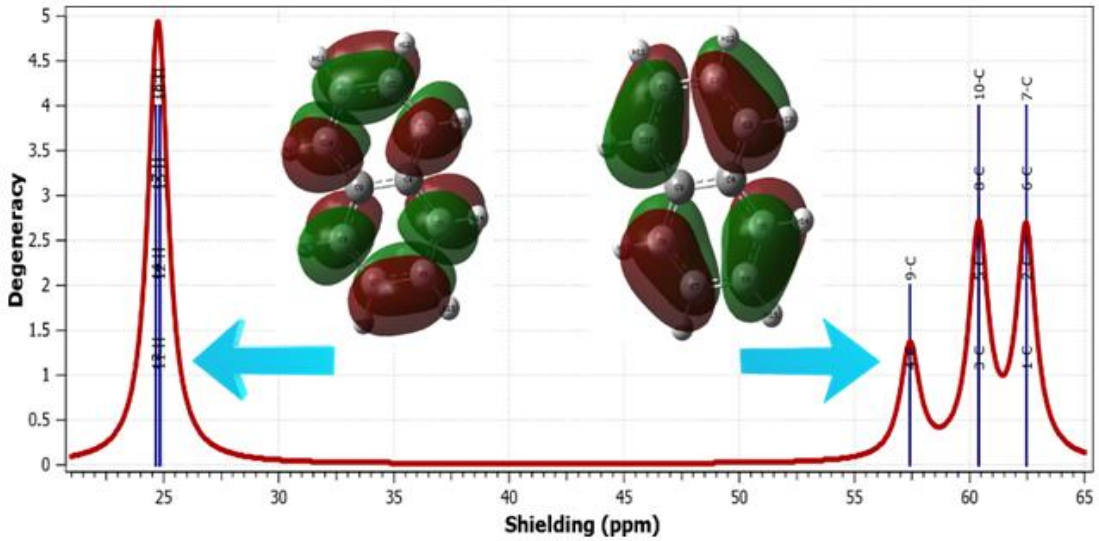

Figure 6. NMR method for naphthalene

UV-visible analysis

Quantitative and qualitative analysis of chemicals, as well as structural determination, are typical uses for ultraviolet (UV) spectroscopy. DFT was used in this investigation, together with the calculational procedures of RB3LYP/ DFT and the 3-21G basis set depicted, (Figure 7). However, the theoretical results of UV spectroscopy were done on Naphthalene. UV Spectroscopy of Naphthalene was also used to probe the maximum excitation energy at a wavelength of 279.29 nm and to quantify the oscillator strength at 96215.95975.

Optical investigation

In this research, DFT was applied, in addition to the calculational optical band gap energy, refractive index, optical density, and optical conductivity using RB3LYP/DFT and the 3-21G basis set that was illustrated below. On the other hand, the theoretical findings of UV spectroscopy were put to use in the examination of the energy band gap in naphthalene. The Tauc plot is widely recognized as a valuable tool in the fields of materials science and solid-state physics. It serves the purpose of obtaining crucial information about the energy band structure of semiconductors and insulators from their optical absorption spectra. The citation encompasses vital information about the reaction conditions, solvents, and reagents, all of which are required for faithfully reproducing the synthesis procedure.

The utilization of Tauc plot analysis enables researchers to acquire valuable insights into the

underlying electronic properties of materials, hence easing the process of material design and optimization for a wide range of technological applications. The Tauc plot is a valuable tool for comprehending and exploiting the electronic properties of various materials, whether they are newly synthesized compounds or already established substances. It enables researchers to investigate the optoelectronic behavior of these materials and refine their qualities, making it a trustworthy and versatile technique in materials science. In this study, we have employed this model to compute both the direct energy band gap and the indirect forbidden energy, as illustrated in Figure 8a **and** 8b.

Future studies can investigate the effect of derivatives on the optical properties of naphthalene. Derivatives of naphthalene, such as substituted naphthalene, have been shown to exhibit different optical properties compared to the parent compound. For example, the absorption spectra of naphthalene derivatives

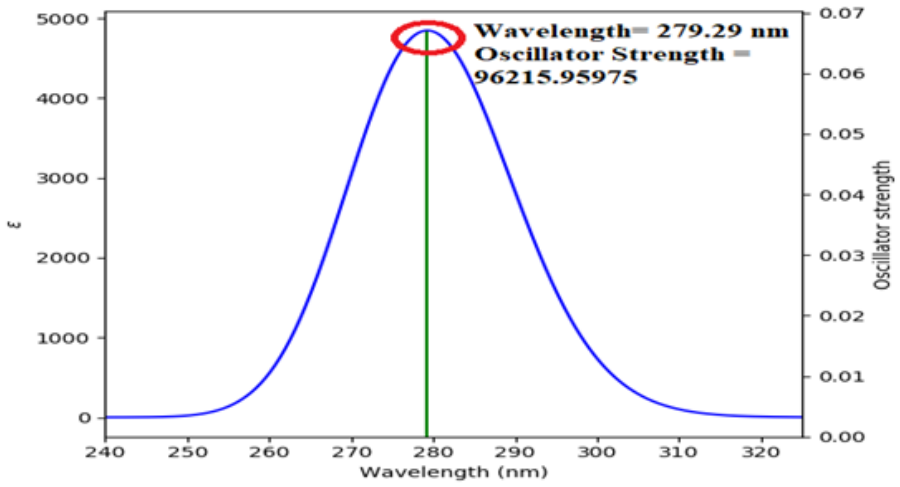

Figure 7. UV-Visible analysis for naphthalene

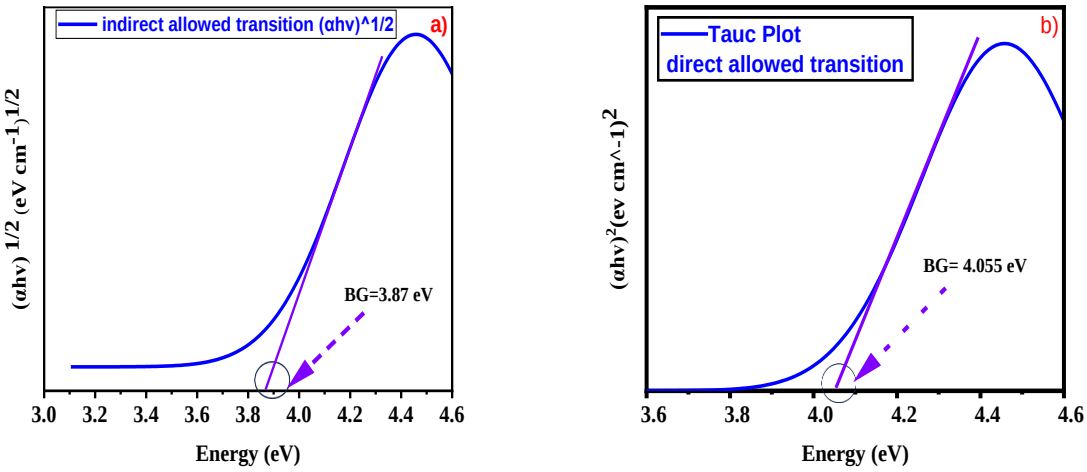

Figure 8. Optical BG a) the indirect transition, b) the direct transition using Tauc plot

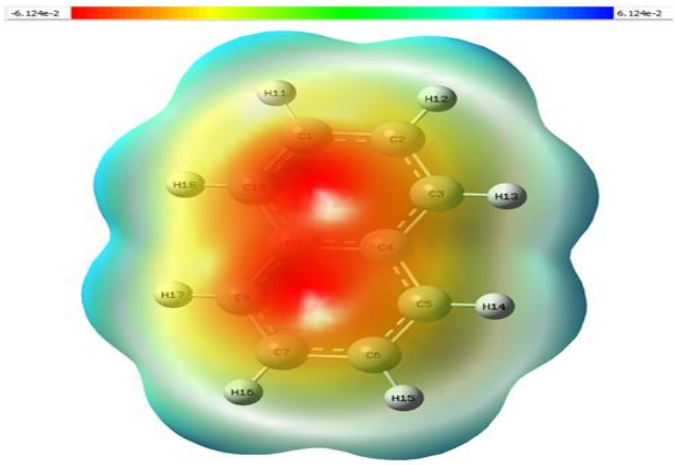

Figure 9. Potential energy map naphthalene

can shift to longer or shorter wavelengths depending on the nature and position of the substituent.

Potential energy map

A potential energy map, also known as a potential energy surface (PES), is a graphical representation of the potential energy of a system of particles as a function of their positions in space [39-41]. It is commonly used in the fields of physics and chemistry to study the behavior of molecules, atoms, and other particles. Various hues in Figure 9 about Naphthalene ($C_{10}H_8$) represent different electrostatic potentials on the molecule's surface. This map's color scheme is a perfect reflection of the range of light we can see. The negatively charged regions of the molecule (those with electrophilic reactivity) are shown in red. A positive charge (nucleophilic reactivity) is shown by the blue area. Colors with the most negative electrical potential (EP) are red, followed by orange, yellow, green, and finally blue.

Areas that are blue tend to have a lower electron density, a bigger positive charge, and a weaker proton affinity. The green range represents nucleophilic reactivity while the blue range represents electrophilic activity. To highlight fields with the most negative electrostatic potential, we use the color red.

Density of states (DOS)

Density-of-state (DOS) plots for the investigated Naphthalene molecule ($C_{10}H_8$) at B3LYP6-31G(d) are shown in Figure 10. The HOMO and LUMO are shown as the (green line and red line), respectively. The distance between green and red lines represents the energy difference between HOMO and LUMO levels for all elements. Further, a comparison of the DOS diagrams reveals that the HOMO and LUMO energies are equally dispersed among all the components under consideration. The density of HOMO states in all the substances under study may be seen using a density of state diagrams. All of the compound distributions point to the contributing components having a greater LUMO density than the center element. The density shift from the source areas to the center region is a property shared by all compounds, as seen by the DOS maps. One can utilize the provided equation 12 to calculate the Density of States (DOS) as a function of energy levels. This equation is expressed as [30,42-45]:

$$DOS(E) = \Sigma\, g(E - \varepsilon_i) \quad (12)$$

In this formula, E represents the total electron energy, 'g' corresponds to a Gaussian function

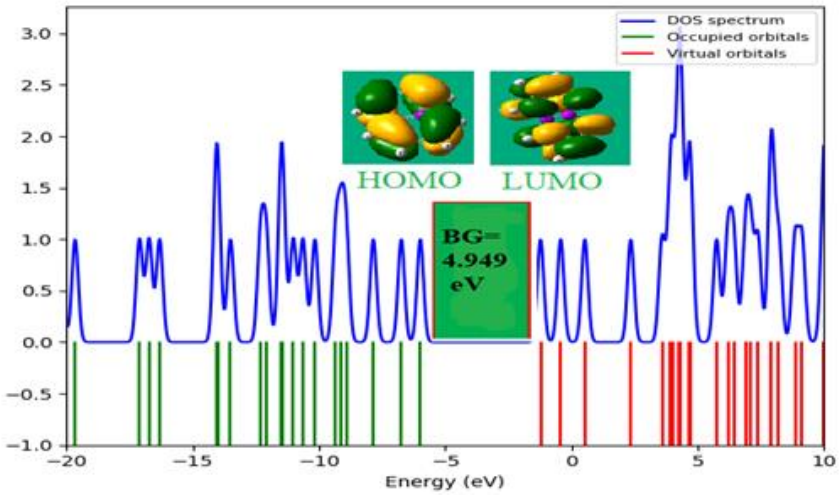

Figure 10. Density of States (DOS) of naphthalene

with a fixed Full Width at Half Maximum (FWHM) of =0.3, and ε_i signifies the energy associated with the i^{th} orbitals. The calculations were conducted using an appropriate DFT approach to ensure an accurate assessment of the Band Gap (BG), which was determined to be 4.949 eV for the 3-21G basis set. This result agrees with literature study [17,46,47]. The manuscript's quantum computing study of naphthalene has promising practical implications in many areas, including drug discovery and design, computational chemistry tools, environmental impact assessment, and material design and development.

Conclusion

In conclusion, the DFT calculations also showed that the lowest energy excited state of naphthalene is a singlet state, while the HF calculations predicted that the lowest energy excited state is a triplet state. This study investigated the structure and properties of naphthalene using density functional theory (DFT) and Hartree-Fock (HF) methods, with a focus on natural bond orbital (NBO) analysis. The NBO analysis of the DFT calculations showed that the bonding in naphthalene is dominated by delocalized pi bonds. The pi bonds are formed by the overlap of the p orbitals of the carbon atoms.

The sigma bonds between the carbon atoms are also important, but they are not as delocalized as the pi bonds. The NBO analysis of the HF calculations showed that the bonding in naphthalene is less delocalized than the DFT calculations. The FT-IR spectra of naphthalene were calculated using both the DFT and HF methods. The DFT calculations were able to reproduce the experimental FT-IR spectra more accurately than the HF calculations. This is because the DFT methods take into account electron correlation, which is important for describing the vibrations of molecules. The DFT calculations showed that the most intense bands in the FT-IR spectrum of naphthalene are due to the stretching vibrations of the C-H bonds. The other bands in the spectrum are due to the bending vibrations of the C-H bonds, the C-C bonds, and the ring breathing mode. The NMR spectra of naphthalene were calculated using both the DFT and HF methods. This is because the DFT methods take into account electron correlation, which is important for describing the magnetic properties of molecules. The DFT calculations showed that the first absorption band in the UV-Visible spectrum of naphthalene is due to the transition from the ground state to the initial excited singlet state.

The other bands in the spectrum are due to higher energy transitions. The researchers recommend that this work may be used to create novel methodologies for the design and synthesis of naphthalene derivatives, and they propose that this be done. The results showed

that the DFT methods gave a more accurate description of the structure and properties of naphthalene than the HF methods. The present research's HOMO-LUMO energy is in conform with a previous DFT investigation on a naphthalene molecule 4.823 eV. The results of this study can be used to develop new methods for the detection and removal of naphthalene from the environment.

Acknowledgements

We express our gratitude to the leaders of Halabja University's physics departments for their assistance.

Orcid

Othman Abdulrahman Hamad
https://orcid.org/0000-0001-8170-9094

Rebaz Obaid Kareem
https://orcid.org/0000-0001-6273-1309

Yousif Hussein Azeez
https://orcid.org/0000-0001-5357-7856

Mehmet Hanifi Kebiroğlu
https://orcid.org/0000-0002-6764-3364

Rebaz Anwar Omer
https://orcid.org/0000-0002-3774-6071

Osama Ismail Haji Zebari
https://orcid.org/0000-0003-4547-6961

References

[1]. R. Lu, J. Wu, R.P. Turco, A.M. Winer, R. Atkinson, J. Arey, S.E. Paulson, F.W. Lurmann, A.H. Miguel, A. Eiguren-Fernandez, Naphthalene distributions and human exposure in Southern California, *Atmospheric Environment*, **2005**, *39*, 489-507. [Crossref], [Google Scholar], [Publisher]

[2]. S. Makar, T. Saha, S.K. Singh, Naphthalene, a versatile platform in medicinal chemistry: sky-high perspective, *European Journal of Medicinal Chemistry*, **2019**, *161*, 252-276. [Crossref], [Google Scholar], [Publisher]

[3]. S.V. Bhosale, C.H. Jani, S.J. Langford, Chemistry of naphthalene diimides, *Chemical Society Reviews*, **2008**, *37*, 331-342. [Crossref], [Google Scholar], [Publisher]

[4]. C. Jia, S. Batterman, A critical review of naphthalene sources and exposures relevant to indoor and outdoor air, *International Journal of Environmental Research and Public Health*, **2010**, *7*, 2903-2939. [Crossref], [Google Scholar], [Publisher]

[5]. R. Goldstein, H.H. Cho, A review of mass transfer measurements using naphthalene sublimation, *Experimental Thermal and Fluid Science*, **1995**, *10*, 416-434. [Crossref], [Google Scholar], [Publisher]

[6]. O. Rebaz, R.F. Rashid, K. Othman, Exploring the synthesis of 1, 2, 4-triazole derivatives: A comprehensive review, *Journal of Physical Chemistry and Functional Materials*, *6*, 43-56. [Crossref], [Google Scholar], [Publisher]

[7]. A. Buckpitt, B. Boland, M. Isbell, D. Morin, M. Shultz, R. Baldwin, K. Chan, A. Karlsson, C. Lin, A. Taff, Naphthalene-induced respiratory tract toxicity: metabolic mechanisms of toxicity, *Drug Metabolism Reviews*, **2002**, *34*, 791-820. [Crossref], [Google Scholar], [Publisher]

[8]. C.S. McEnally, L.D. Pfefferle, Improved sooting tendency measurements for aromatic hydrocarbons and their implications for naphthalene formation pathways, *Combustion and Flame*, **2007**, *148*, 210-222. [Crossref], [Google Scholar], [Publisher]

[9]. B. Mohapatra, P.S. Phale, Microbial degradation of naphthalene and substituted naphthalenes: metabolic diversity and genomic insight for bioremediation, *Frontiers in Bioengineering and Biotechnology*, **2021**, *9*, 602445. [Crossref], [Google Scholar], [Publisher]

[10]. E.R. Lippincott, E.J. O'Reilly Jr, Vibrational spectra and assignment of naphthalene and naphthalene-d-8, *Journal of Chemical Physics*, **1955**, *23*, 238-244. [Crossref], [Google Scholar], [Publisher]

[11]. P. Rai, K. Maji, S.K. Jana, B. Maji, Intermolecular dearomative [4+2] cycloaddition of naphthalenes via visible-light energy-transfer-catalysis, *Chemical Science*, **2022**, *13*, 12503-12510. [Crossref], [Google Scholar], [Publisher]

[12]. O. Rebaz, L. AHMED, H. Jwameer, P. KOPARIR, Structural analysis of epinephrine by combination of density functional theory and hartree-fock methods, *El-Cezeri*, **2021**, *9*, 760-776. [Crossref], [Google Scholar], [Publisher]

[13]. W.F. Guerin, S.A. Boyd, Differential bioavailability of soil-sorbed naphthalene to two bacterial species, *Applied and Environmental Microbiology*, **1992**, *58*, 1142-1152. [Crossref], [Google Scholar], [Publisher]

[14]. U. Pandya, M.K. Saini, G.F. Jin, S. Awasthi, B.F. Godley, Y.C. Awasthi, Dietary curcumin prevents ocular toxicity of naphthalene in rats, *Toxicology Letters*, **2000**, *115*, 195-204. [Crossref], [Google Scholar], [Publisher]

[15]. R. Anwar Omar, P. Koparir, M. Koparir, D.A. Safin, A novel cyclobutane-derived thiazole–thiourea hybrid with a potency against COVID-19 and tick-borne encephalitis: Synthesis, characterization, and computational analysis, *Journal of Sulfur Chemistry*, **2024**, *45*, 120-137. [Crossref], [Google Scholar], [Publisher]

[16]. K.M. Yen, C.M. Serdar, I.C. Gunsalus, Genetics of naphthalene catabolism in pseudomonads, *CRC Critical Reviews in Microbiology*, **1988**, *15*, 247-268. [Crossref], [Google Scholar], [Publisher]

[17]. O. Rebaz, P. Koparir, I. Qader, L. Ahmed, Theoretical determination of corrosion inhibitor activities of naphthalene and tetralin, *Gazi University Journal of Science*, **2022**, *35*, 434-444. [Crossref], [Google Scholar], [Publisher]

[18]. S.A. Siadati, E. Vessally, A. Hosseinian, L. Edjlali, Possibility of sensing, adsorbing, and destructing the Tabun-2D-skeletal (Tabun nerve agent) by C20 fullerene and its boron and nitrogen doped derivatives, *Synthetic Metals*, **2016**, *220*, 606-611. [Crossref], [Google Scholar], [Publisher]

[19]. E. Vessally, S.A. Siadati, A. Hosseinian, L. Edjlali, Selective sensing of ozone and the chemically active gaseous species of the troposphere by using the C_{20} fullerene and graphene segment, *Talanta*, **2017**, *162*, 505-510. [Crossref], [Google Scholar], [Publisher]

[20]. H. Jouypazadeh, H. Farrokhpour, E. Vessally, The adsorption of sulfur mustard chemical warfare agent on the $Ga_{12}N_{12}$ and $Ca_{12}O_{12}$ nanocages; A systematic DFT study, *Computational and Theoretical Chemistry*, **2023**, *1230*, 114358. [Crossref], [Google Scholar], [Publisher]

[21]. H. Jouypazadeh, S. Arshadi, B.C. Panduro, A. Kumar, S. Habibzadeh, S. Ahmadi, E. Vessally, Metalloporphyrin reduced C_{70} fullerenes as adsorbents and detectors of ethenone; A DFT, NBO, and TD-DFT study, *Journal of Molecular Graphics and Modelling*, **2023**, *122*, 108481. [Crossref], [Google Scholar], [Publisher]

[22]. E. Vessally, M. Hosseinali, M.R. Poor Heravi, B.J.J.o.S.C. Mohammadi, DFT study of the adsorption of simple organic sulfur gases on *g*-C_3N_4; periodic and non-periodic approaches, *Journal of Sulfur Chemistry*, **2023**, *44*, 733-50. [Crossref], [Google Scholar], [Publisher]

[23]. H. Kebiroglu, O.A. Hamad, O. Kaygili, N. Bulut, Epinephrine compound: Unveiling its optical and thermochemical properties via quantum computation methods, SSRN, **2023**. [Crossref], [Google Scholar], [Publisher]

[24]. T. Mohr, V. Aroulmoji, R.S. Ravindran, M. Müller, S. Ranjitha, G. Rajarajan, P. Anbarasan, DFT and TD-DFT study on geometries, electronic structures and electronic absorption of some metal free dye sensitizers for dye sensitized solar cells, *Spectrochimica Acta Part A: Molecular and Biomolecular Spectroscopy*, **2015**, *135*, 1066-1073. [Crossref], [Google Scholar], [Publisher]

[25]. S.A. Siadati, Effect of steric congestion on the stepwise character and synchronicity of a 1, 3-dipolar reaction of a nitrile ylide and an olefin, *Journal of Chemical Research*, **2015**, *39*, 640-644. [Crossref], [Google Scholar], [Publisher]

[26]. J.L. Gázquez, A. Cedillo, A. Vela, Electrodonating and electroaccepting powers, *Journal of Physical Chemistry A*, **2007**, *111*, 1966-1970. [Crossref], [Google Scholar], [Publisher]

[27]. D.M. Mamand, Y.H. Azeez, H.M. Qadr, Monte Carlo and DFT calculations on the corrosion inhibition efficiency of some benzimide molecules, *Mongolian Journal of Chemistry*, **2023**, *24*. [Crossref], [Google Scholar], [Publisher]

[28]. H.H. Rasul, D.M. Mamad, Y.H. Azeez, R.A. Omer, K.A.J.C. Omer, T. Chemistry, Theoretical investigation on corrosion inhibition efficiency of some amino acid compounds, *Computational and Theoretical Chemistry*, **2023**, *1225*, 114177. [Crossref], [Google Scholar], [Publisher]

[29]. M. El Idrissi, S. Elharfaoui, Z. Zmirli, A. Mouhssine, A. Dani, B. Salle, A. Tounsi, K. Digua, H. Chaair, Theoretical and experimental study of the orientation to the most effective coagulant for removing reactive black-5 dye from industrial effluents, *Physical Chemistry Research*, **2024**, *12*, 229-248. [Crossref], [Google Scholar], [Publisher]

[30]. O. Hamad, R.O. Kareem, O. Kaygili, Density function theory study of the physicochemical characteristics of 2-nitrophenol, *Journal of Physical Chemistry and Functional Materials*, **2023**, *6*, 70-76. [Crossref], [Google Scholar], [Publisher]

[31]. M. Sucheta, A. Pramod, M. Zikriya, K.M. Salma, N. Venugopal, R. Chaithra, D. Harshitha, S. Amudan, C. Renuka, S. Murthy, Frontier molecular orbital, molecular structure and Thermal properties of 2, 4, 6, 8-tetramethyl-2, 3, 6, 7-tetrahydro-s-indacene-1, 5-dione using DFT calculation, *Materials Today: Proceedings*, **2022**, particle in partially filled Landau levels, *Physical Review Letters*, **2021**, *126*, 156802. [Crossref], [Google Scholar], [Publisher]

[38]. A.E. Parlak, R.A. Omar, P. Koparir, M.I. Salih, Experimental, DFT and theoretical corrosion study for 4-(((4-ethyl-5-(thiophen-2-yl)-4*H*-1, 2, 4-triazole-3-yl) thio) methyl)-7, 8-dimethyl-2*H*-chromen-2-one, *Arabian Journal of* *62*, 5241-5244. [Crossref], [Google Scholar], [Publisher]

[32]. N.M. O'boyle, A.L. Tenderholt, K.M. Langner, Cclib: a library for package-independent computational chemistry algorithms, *Journal of Computational Chemistry*, **2008**, *29*, 839-845. [Crossref], [Google Scholar], [Publisher]

[33]. H. Shahab, Y. Husain, Theoretical study for chemical reactivity descriptors of tetrathiafulvalene in gas phase and solvent phases based on density functional theory, *Passer Journal of Basic and Applied Sciences*, **2021**, *3*, 167-173. [Crossref], [Google Scholar], [Publisher]

[34]. S. Hekim, Y.H. Azeez, S. Akpinar, The theoretical investigation of the HOMO, LUMO energies and chemical reactivity of C_9H_{12} and $C_7F_3NH_5Cl$ molecules, *Journal of Physical Chemistry and Functional Materials*, **2019**, *2*, 29-31. [Crossref], [Google Scholar], [Publisher]

[35]. C.-G. Zhan, J.A. Nichols, D.A. Dixon, Ionization potential, electron affinity, electronegativity, hardness, and electron excitation energy: molecular properties from density functional theory orbital energies, *Journal of Physical Chemistry A*, **2003**, *107*, 4184-4195. [Crossref], [Google Scholar], [Publisher]

[36]. F. Sessa, M. Rahm, Electronegativity equilibration, *Journal of Physical Chemistry A*, **2022**, *126*, 5472-5482. [Crossref], [Google Scholar], [Publisher]

[37]. F. Yang, A.A. Zibrov, R. Bai, T. Taniguchi, K. Watanabe, M.P. Zaletel, A.F.J.P.r.l. Young, Experimental determination of the energy per

Chemistry, **2022**, *15*, 104088. [Crossref], [Google Scholar], [Publisher]

[39]. D.M. Mamad, R.A. Omer, K.A. Othman, Quantum chemical analysis of amino acids as anti-corrosion agents, *Corrosion Reviews*, **2023**, *41*, 703-17. [Crossref], [Google Scholar], [Publisher]

[40]. D.M. Mamad, H.H. Rasul, A.H. Awla, R.A. Omer, Insight into corrosion inhibition efficiency of imidazole-based molecules: A quantum chemical study, *Doklady Physical Chemistry,* **2023**, *511*, 125-133. [Crossref], [Google Scholar], [Publisher]

[41]. H.H. Rasul, D.M. Mamad, Y.H. Azeez, R.A. Omer, K.A. Omer, Theoretical investigation on corrosion inhibition efficiency of some amino acid compounds, *Computational and Theoretical Chemistry*, **2023**, 114177. [Crossref], [Google Scholar], [Publisher]

[42]. F. İsen, O. Kaygili, N. Bulut, T. Ates, F. Osmanlıoğlu, S. Keser, B. Tatar, İ. Özcan, B. Ates, F. Ercan, Experimental and theoretical characterization of Dy-doped hydroxyapatites, *Journal of the Australian Ceramic Society*, **2023**, 59, 849-864. [Crossref], [Google Scholar], [Publisher]

[43]. R.O. Kareem, O. Kaygili, T. Ates, N. Bulut, S. Koytepe, A. Kuruçay, F. Ercan, I. Ercan, Experimental and theoretical characterization of Bi-based hydroxyapatites doped with Ce, *Ceramics International*, **2022**, *48*, 33440-33454. [Crossref], [Google Scholar], [Publisher]

[44]. A.A. Korkmaz, L.O. Ahmed, R.O. Kareem, H. Kebiroglu, T. Ates, N. Bulut, O. Kaygili, B. Ates, Theoretical and experimental characterization of Sn-based hydroxyapatites doped with Bi, *Journal of the Australian Ceramic Society*, **2022**, *58*, 803-815. [Crossref], [Google Scholar], [Publisher]

[45]. R.O. Kareem, O. Kaygili, Synthesis and Characterization of Bismuth-based hydroxyapatites doped with cerium, Master's Thesis, **2023**. [Crossref], [Google Scholar]

[46]. G. Venkatesh, Y. Sheena mary, Y. Shymamary, V. Palanisamy, M. Govindaraju, Quantum chemical calculations and molecular docking studies of some phenothiazine derivatives, *Journal of Applied Organometallic Chemistry*, **2021**, *1*, 148-158. [Crossref], [Google Scholar], [Publisher]

[47] F.A. Rad. J.T. Mehrabad. M.D. Esrafili, A communal experimental and DFT study on structural and photocatalytic properties of nitrogen-doped TiO_2, *Advanced Journal of Chemistry, Section A*, **2023**, *6*, 244-252. [Crossref], [Google Scholar], [Publisher]